

Particle tracking in living cells: a review of the mean square displacement method and beyond

Naama Gal · Diana Lechtman-Goldstein ·
Daphne Weihs

Received: 16 September 2012 / Revised: 29 January 2013 / Accepted: 7 February 2013 / Published online: 12 March 2013
© Springer-Verlag Berlin Heidelberg 2013

Abstract The focus of many particle tracking experiments in the last decade has been active systems, such as living cells. In active systems, the particles undergo simultaneous active and thermally driven transport. In contrast to thermally driven transport, particle motion driven by active processes cannot directly be correlated to the rheology of the probed region. The rheology in particle tracking experiments is typically obtained through the mean square displacements (MSD) of the trajectories. Hence, the MSD and its functional form remain the only basic tools to evaluate and compare living cells or other active systems. However, the mechano-structural characteristics of the intracellular environment and the mechanisms driving particle transport cannot be revealed by the MSD alone. Hence, approaches for advanced analysis of particle trajectories have been introduced recently. Here, we present a broad review of the extensive intracellular particle tracking experiments that have been carried out on a wide variety of cell types. Those works utilize the MSD, revealing similarities and differences relating to cell type and experimental setup. We also highlight several advanced trajectory-and displacement-based analysis methods and illustrate their capabilities using particle tracking data obtained from two cancer cell lines. We show that combining these analysis methods with the MSD can reveal additional information on intracellular structure and the existence and nature of active processes driving particle motion in cells.

Keywords Particle tracking · Mean square displacement · Trajectory analysis · Intracellular mechanics

Introduction

In active systems such as living cells, the mean square displacements (MSD) of particle motion cannot directly be correlated with rheological parameters, such as the creep compliance and dynamic moduli (Bursac et al. 2005; Mizuno et al. 2007; Wilhelm 2008). Deduction of rheological parameters from the MSD requires the generalized Stokes–Einstein–Sutherland relation, developed under the assumption of exclusively thermal driving forces (Einstein 1905; Mason and Weitz 1995; Squires and Brady 2005; Sutherland 1905); in fact, the generalization also requires the material to be a (hydrodynamic) continuum, homogeneous, isotropic, and incompressible (Squires and Mason 2010). Driving forces in cells are, however, a combination of thermal fluctuations and active contributions from motor transport and cytoskeleton remodeling, leading to system far from equilibrium (Hoffman et al. 2006; Mizuno et al. 2007; Weihs et al. 2006). Hence, several methods have recently been suggested to augment the MSD and reveal processes driving particle motion in the dynamic intracellular microenvironment.

Here, we review and discuss particle tracking results in living cells and what has been revealed from such experiments to date using the MSD. The MSD has revealed active transport and dynamics in cells. Analysis going beyond the MSD can suggest mechanisms driving particle transport, and we highlight several such approaches for advanced trajectory analysis. The approaches presented here can be applied to any particle tracking experiment, active or thermally driven. The structure of the manuscript is as follows: first, we provide a basic description of the mechanical

Special issue devoted to novel trends in rheology.

N. Gal · D. Lechtman-Goldstein · D. Weihs (✉)
Faculty of Biomedical Engineering, Technion-Israel Institute
of Technology, Haifa 32000, Israel
e-mail: daphnew@tx.technion.ac.il

elements of the cell, followed by discussion of techniques that have been used to measure whole cell and extracellular mechanics through response to force application. We then explain the basic approach for particle tracking microrheology with the MSD as a basic tool and discuss specific issues arising when applying particle tracking in cells. We specifically consider conditions under which intracellular rheology may still be obtained from particle tracking data. Following that, we provide an in-depth discussion of the current state of the field, through a broad compilation of intracellular particle tracking works carried out in the last decade. We focus on the observed MSD and MSD scaling exponents and discuss apparent similarities and differences depending on cell type and experimental setup. Finally, as an extension to the commonly utilized MSD, we highlight several recently suggested methods for advanced trajectory analysis. Those are designed to augment the MSD and provide more information on the underlying mechanisms driving particle transport in cells. We illustrate each of the methods with data obtained from two cancer cell lines—high and low metastatic potential. We use our results to simultaneously show what can be obtained with each of the methods as well as to expose and discuss differences in intracellular structure and mechanics between the two cell types.

Cell structure and the cytoskeleton

Cells are required to dynamically change shape and apply forces during normal function, such as division, adherence, and motility. Those capabilities require continuous regulation and remodeling, affecting intracellular structure and mechanics. The internal microenvironment of living cells is a collection of compartments with specific functionalities located within a crowded and viscoelastic cytoplasm. The viscoelasticity of the cytoplasm largely results from the cytoskeleton which stabilizes and facilitates many dynamic processes in the cell. The dynamic abilities and viscoelasticity of the cytoskeleton result mostly from active remodeling and interactions with associated molecular motors. Motors form dynamic and adaptive cytoskeletal networks that can be restructured and moved according to cell function. The cytoskeletal networks have three main functions: spatially organizing the cell contents, connecting the cell physically and biochemically to its external environment, and generating coordinated forces that enable the cell to move and change shape (Fletcher and Mullins 2010).

The concentration and molecular architecture of the different components of the cytoskeleton determine the overall deformability and mechanical response of the cell (Heidemann and Wirtz 2004; Janmey and Weitz 2004). That response combines force application capabilities which are part of the interactions with neighboring cells and the extracellular matrix.

The cytoskeleton is composed of three main components: actin filaments, microtubules, and intermediate filaments. Actin is typically associated with dynamic processes, such as motility and adhesion, and is concentrated at the cell periphery, close to the membrane. Actin filaments in cells are normally arranged into bundles or networks. Networks can form when myosin molecular motors crosslink actin filaments. The actomyosin network is highly dynamic and can be used to transport cargo and also apply contractile forces. Forces are generated as myosin slides filaments against each other thus creating tension (Pollard and Cooper 2009).

Microtubules are primarily abundant deep inside the cell yet span from the nucleus to the membrane. Microtubules are involved in various functions such as cell division, intracellular transport, and cell morphogenesis and organization. Intracellular transport and organization are facilitated by two families of molecular motors, kinesin and dynein that travel to and from the membrane, respectively (Valiron et al. 2001). The role of microtubules in structural stability and transport requires slower dynamics where their disassembly time is typically minutes to hours. Intermediate filaments (IFs) are the most structurally diverse of the three building blocks of the cytoskeleton, as over 40 separate types of intermediate filaments have been identified with cell-type-specific expression. Their major function is assumed to be that of mechanical stress absorber and an integrating device for the entire cytoskeleton (Herrmann et al. 2007; Nagle 1994).

The cytoskeleton and the cell membrane are the main mechanical elements of the cell. They allow cells to mechanically adapt to changing environments and applied forces. The mechanical response of cells and their cytoskeleton has been evaluated using a variety of techniques.

Tools for active extracellular mechanics measurements

In the past decade, increasing attention has been drawn to the fascinating interplay between biological function and mechano-structural responses of cells. The reciprocity between mechanics and function affects many normal cellular processes, such as differentiation, proliferation, motility, and programmed cell death (Discher et al. 2009; Huang and Ingber 1999; Lim et al. 2006; Suresh et al. 2005). For example, cells respond to variations in stiffness of their environment by changing their morphology, differentiated state, and even forces that they are able to apply (Cameron et al. 2011; Discher et al. 2005; Engler et al. 2006; Zemel et al. 2010). Such changes are associated with membrane restructuring and cytoskeleton remodeling (Discher et al. 2005). Cortex-region mechanics can be accessed through external or whole cell measurements. The measured elastic modulus of a single cell is orders of magnitude lower than

that of materials like metals, ceramics, and even polymers (Bao and Suresh 2003; Chen et al. 2010). Experimental techniques capable of probing forces and displacements on sub-pico Newton and sub-nanometer scales are required. The evolution of experimental techniques for such small-scale mechanical measurements is largely responsible for the considerable progress in cellular biomechanics research.

Many methods have recently been developed to measure the mechanical response of a single cell to an applied force or stress, similar to rheometry. In those methods, forces are applied either to the entire cell or to localized regions on the membrane, providing a measure of whole cell compliance or local viscoelasticity, respectively. Induced deformations on the cell as a whole can provide estimation of the cell compliance through changes in cell size and shape. Such techniques include microplate stretchers (Asnacios et al. 2006; Suresh et al. 2005; Thoumine et al. 1999), an optical stretcher (Guck et al. 2005), microfluidics devices (Hou et al. 2009; Qi et al. 2012), micropipette aspiration (Evans et al. 1995; Guo et al. 2012), applied shear flow, or substrate stretching (Suresh 2007). In contrast, other methods have been developed that probe regions at the cell membrane, typically at contact points with the cytoskeleton.

The viscoelastic response of the cortical cytoskeleton can be accessed by applying force at localized regions on the cell membrane. Force is applied to the membrane and the adjoining cytoskeleton using beads or cantilevers, which also serve as probes for the mechanical response. Those probes can interact with the cytoskeleton through the membrane or estimate the combined cytoskeleton–membrane response of a region. The combined response can be obtained by applying small deformation to the membrane using, for example, atomic force microscopy (Binnig et al. 1986; Chaudhuri et al. 2009; Cross et al. 2007). In contrast, responses of the cytoskeleton to extension and torsion have been measured by beads connected to the actin cytoskeleton through membrane-traversing integrins. Beads biochemically attached to the cytoskeleton can be rotated in magnetic twisting cytometry (Fabry et al. 2001; Puig-de-Morales et al. 2001) or pulled by magnetic or optical tweezers (Bausch et al. 1998; Tanase et al. 2007; Van Vliet et al. 2003; Zhang and Liu 2008). In such experiments, the relative contribution of endogenous active forces in cells can be evaluated by combining “passive” tracking and active manipulation of probes (Gallet et al. 2009; Hoffman et al. 2006; Mizuno et al. 2007). However, this does not provide information on the specific elements in the cell driving the active motion.

Rheometry-like stress application is more difficult inside living cells. Applying force inside cells can easily disrupt the internal structure in an abnormal way, making analysis difficult. With very few exceptions (de Vries et al. 2005; Robert et al. 2010; Wilhelm 2008), active methods have

only been used to probe response of the cortex or a whole cell, where the cell interior remains largely inaccessible to such approaches. However, intracellular mechanics provide an important measure of the internal structural response that can occur in parallel with observed external changes. Notably, the internal response may not intuitively match the external one, underscoring the importance of both types of studies. For example, the external and internal mechanics of mouse fibroblasts were concurrently evaluated following microtubule network disruption. Following microtubule disruption, the Young’s modulus of the cortex reduced by 80 % (Pelling et al. 2007), while the internal microenvironment exhibited stiffening on similar time scales (Weihs et al. 2007a). That indicates a cascade of biochemical and mechanical changes occurring throughout the cell. To evaluate changes and responses of intracellular microenvironments in real time, particle tracking is currently the method of choice and the only approach that does not introduce external stresses to the system.

Early particle tracking microrheology experiments were already performed in the 1920s where magnetic particles were actively manipulated within gelatin to reveal the qualitative response of the viscoelastic materials (Freundlich and Seifriz 1923; Heilbronn 1922). This approach was also later implemented to the cell cytoplasm (Crick and Hughes 1950; Hiramoto 1969a, b; Yagi 1961) and to mucus (King and Macklem 1977). Those measurements, however, could not provide precise evaluation of sample rheology due to past limitations in probe design, particle tracking, and motion analysis (MacKintosh and Schmidt 1999). Current experiments are predominately “passive”, where no external force is applied to move the particles.

Particle tracking microrheology

Particle motion is often characterized by the estimator to the second moment of the displacement, through the time-averaged mean square displacement. The MSD is a statistical measure of time-dependent particle displacements $\langle \Delta r^2(\tau) \rangle = \langle |r(t+\tau) - r(t)|^2 \rangle_t$, where $r(t)$ and $r(t+\tau)$ are the positions of a single particle at two time points τ seconds apart. The angular brackets in the MSD indicate a time average on all such position pairs in a trajectory. Fewer pairs are available for averaging at long lag times, which reduces statistics, and can result in wavy MSD plots. To improve the statistics especially at longer lag times, the MSD may also be provided as simultaneous time and ensemble averages of several particles. It is important to note that time averaging is applicable only when assuming a stationary transport processes (Mason et al. 1997b). For example, Brownian diffusion is stationary, yet if an underlying constant drift-velocity exists, perhaps due to cell crawling,

the process will become non-stationary. Random diffusion (Brown 1828) occurs under thermal equilibrium, when only thermal energy is available to drive particle motion; thermal energy is on the order of $k_B T$ where k_B is Boltzmann's constant and T is the absolute temperature. Under thermal equilibrium, the rheology of a microscale region in a system can be obtained through the motion of particles and the resulting MSD.

A particle randomly moving in a viscous, thermally equilibrated, d -dimensional system will exhibit linear time dependence of the MSD: $\langle \Delta r^2(\tau) \rangle = 2dD\tau$. The MSD depends on the diffusion coefficient, D , which is a measure for the rate that a particle of radius R_p can move through a fluid of viscosity, η . For a system at thermal equilibrium, the diffusion coefficient is given by the Stokes–Einstein–Sutherland relation $D = k_B T / 6\pi\eta R_p$, where the particle experiences Stokes drag (Einstein 1905; Sutherland 1905). The same expression was developed in parallel by Einstein and Sutherland, yet it was accredited only to Einstein until recently (Squires and Brady 2005). Thus, the Stokes–Einstein–Sutherland relation directly correlates an obtained MSD with the viscosity for a purely viscous liquid at thermal equilibrium. This relation had been generalized provided the local rheology of non-Newtonian viscoelastic fluids. Thus, the complex shear modulus (Mason et al. 1997b; Mason and Weitz 1995), the creep compliance (Xu et al. 1998), and the dynamic moduli (Dasgupta et al. 2002; Mason 2000) can be determined for non-Newtonian fluids using the MSD.

In the development of the generalized Stokes–Einstein relation, effects of inertia have been neglected (Mason and Weitz 1995). Inertia becomes significant, however, at high enough sampling frequencies or very short time scales and can result in oscillations in the MSD (Indei et al. 2012a, b); the critical resonance frequency is related to the relaxation time of the material. For example, particle tracking with micron-scale tracers in wormlike micelle (Willenbacher et al. 2007) showed a deviation in the loss modulus, $G''(\omega)$ above $\omega = 0.1$ – 1 MHz, when inertia was neglected (Indei et al. 2012b). It is important to note that even at high acquisition rates, the oscillations may not be visible as they are dampened by the solvent viscosity (Head and Mizuno 2010; Indei et al. 2012a). In contrast, at low frequency or long lag times, the inertial effects are negligible, the generalized Stokes–Einstein–Sutherland equation is appropriate, and the MSD can be used to obtain sample rheology.

In viscoelastic systems, the MSD can typically be described by a single or multiple power-law time dependence: $\langle \Delta r^2(\tau) \rangle = A\tau^\alpha$ (Saxton and Jacobson 1997; Weihs et al. 2006). Existence of a power law typically indicates a balance between two contributing forces, such as energy consuming (active) and thermally mediated. The driving

forces together with the particle microenvironment determine the mode-of-motion that will be indicated by the MSD scaling exponent, α . The MSD scaling exponent is the slope of the log-log plot of the time-dependent MSD, and its physical range is $0 \leq \alpha \leq 2$. In a non-active fluid, the scaling exponent is in the range of $0 \leq \alpha \leq 1$, where the extremes represent the elastic (trapped) and viscous (diffusive) limits, respectively. Any intermediate values are termed sub-diffusive and typically indicate hindrance to free diffusion by steric obstacles or by friction resulting from motion through a (continuum) viscoelastic medium. Sub-diffusion can originate from network confinement and friction was shown in semiflexible polymer and in actin networks, where a scaling of 0.75 has been obtained experimentally and theoretically over various lag times (Gittes et al. 1997; Granek 1997; Morse 1998). Similar exponents have been observed at long time scales in living cells, where particle motion indicates cytoskeletal hindrance as the average persistence time on molecular motors is exceeded (Caspi et al. 2000). Transport induced by molecular motors and other active processes result in super diffusion, typically with scaling above unity (at lag times on the order of 1 s), but that may also be close to unity (Brangwynne et al. 2008). Under active transport, the MSD scaling exponent is $0 \leq \alpha \leq 2$, where $\alpha = 2$ is the ballistic limit of pure convection; in pure convection $x = v\tau$ and thus $x^2 = (v\tau)^2$. Thus, the MSD scaling exponent provides an indication to the mode of motion yet cannot reveal the actual mechanisms driving the motion (Burov et al. 2011). The MSD is, nevertheless, the best starting point of particle tracking analysis. A detailed review of the stages in setting up a system for particle tracking and accurately obtaining particle trajectories is provided elsewhere (Crocker and Hoffman 2007).

To obtain the MSD, each particle may be tracked individually, or correlated motion of pairs of close-by particles may be evaluated (Mason et al. 1997a). Two-particle microrheology (Crocker et al. 2000; Levine and Lubensky 2000) is superior when evaluating local rheology, providing results comparable to macroscopic rheology. Both methods can be used to probe microstructure that is larger or smaller than the particle; in the latter, the particle experiences the probed network as a continuum. However, within cells, both single- and two-particle analyses have their advantages and disadvantages (Crocker and Hoffman 2007; Lau et al. 2003; Weihs et al. 2006). The main differences between the approaches are the range of region that is probed and effects of probe–network interactions. Single particle tracking probes the heterogeneities in the immediate region of the particle and is affected by probe interactions with the microenvironment. In contrast, the two-particle approach probes the local bulk region between two particles and removes effects of probe interactions. In cells, it is often

difficult to obtain sufficient statistics for two-particle tracking, especially when using internalized probes, and thus, endogenous granules are often used (Hoffman et al. 2006); those may not be available in all cell types and are often localized only in specific regions in the cells. Hence, most intracellular works utilize single particle tracking to obtain the MSD. It is important to note that the MSD does not easily translate to rheology in cells.

Intracellular particle tracking

The generalized Stokes–Einstein–Sutherland relation cannot automatically be applied to describe particle motion in living cells or in other active systems. In such systems, the assumption that only thermal energy is available to drive particle motion is, of course, violated. In cells, particle motion is driven concurrently by thermal fluctuations and by active processes utilizing intracellular energy sources. Specifically, adenosine-5'-triphosphate (ATP) drives actin remodeling and molecular motor transport, and guanosine-5'-triphosphate (GTP) drives microtubule remodeling. Cytoskeletal remodeling and motor transport can (directly and indirectly) induce particle motion, resulting in displacements that may be larger or more directional than those expected if motion was exclusively thermal in origin (Bursac et al. 2005; Mizuno et al. 2007; Wilhelm 2008). Whether or not rheology can be extracted, the MSD still provides an indication to the mode of motion and to the mechanics of the microenvironment. Specifically, the MSD amplitude was shown to be inversely proportional to the local stiffness in cells (Brangwynne et al. 2009; Hoffman et al. 2006). Thus, for example, comparing the MSDs of cancer cells with increasing metastatic potential has shown an increase in intracellular activity together with a decrease in stiffness and structural density (Gal and Wehs 2012).

It may still be possible to use the generalized Stokes–Einstein–Sutherland relation in living cells under specific conditions. Such conditions include experiments where active cellular processes are inhibited, or if the time scale of observation is shorter than that of the active processes. It has been suggested that a measure of the “passive” mechanics of the cell may be obtained following ATP depletion (Hoffman et al. 2006). This approach, however, may be applicable only when morphological, structural, and viability changes of the cell to ATP depletion are small, which is not the case for many cell types. In addition, it is important to note that ATP depletion does not significantly affect GTP levels in the cell (Schwoebel et al. 2002), and thus, active processes especially in microtubule-rich regions still exist. Another approach to reveal the underlying thermally driven motion is

to acquire data at time scales shorter than those of the active processes. Active modes in cells are typically not dominant at time scales <0.1 s (frequencies >10 Hz), revealing thermally driven processes (Brangwynne et al. 2009; Mizuno et al. 2007). For example, the MSD scaling exponent in drosophila cells is 0.6 for lag times <0.03 s and increases to 1.6 at longer time scales, indicating a shift from thermal to active regimes (Kulic et al. 2008).

It is important to note that a reduction of the MSD scaling exponent below unity may be observed at short times, yet this does not immediately indicate a change in the mode of motion. At short times, the MSD amplitude is typically small and close to the noise floor of the system (Savin and Doyle 2005). The noise floor depends on the mechanical stability of the experimental setup, particle size, magnification, frame rate, tracking algorithm, and other parameters (Cheezum et al. 2001). These system parameters determine the smallest displacement that can reliably be obtained from a specific system. If the MSD is close to the noise floor, it can appear to flatten out, while the system noise is in fact biasing the measurement. Thus, the system noise must be subtracted from the MSD (Savin and Doyle 2005) to avoid artifactual changes in the MSD and the MSD scaling exponents especially at the shortest lag times.

Many particle tracking experiments have been run in the past decade, revealing interesting differences and similarities between mammalian cell types. Table 1 shows a collection of a wide variety of works on 23 different cell types (primarily mammalian), using endogenous, spontaneously endocytosed, or injected particles as probes; all cells were untreated by any chemicals. While this table is by no means a full compilation of the literature, it is representative of the types of cells that were studied and experimental setups that have been used. We have only included single particle tracking works that had explicitly shown the MSD and its scaling exponents.

We observe general differences in the MSD scaling exponents of midrange time scales (0.5–6 s) that depend mainly on the internalization method more than the cell type (Table 1). The internalization method determines particle interaction with the intracellular microenvironment and localization in the cell, i.e., the probed regions. Most endogenous particles have exhibited $\alpha = 0.75$ –1. Ballistic injection and microinjection of probes resulted in α of approximately unity or below it, as a result of non-interacting particles localized into possibly less active regions. Using natural uptake, or endocytosis, we note that in most cases, superdiffusive $\alpha > 1$ were reported, regardless of cell type, particle diameter, frame rate, or tracking method.

Differences between the experimental setups can have great impact on the determined values of the MSD scaling exponent. Hence, we compare the exponents obtained by

Table 1 Compilation of MSD scaling exponents observed in intracellular particle tracking experiments classified according to particle internalization technique

Cell type	Designation	Probes ^a	Tracking method	Frame rate (fps)	Total time (s) ^b	Lag time (s)	MSD scaling exponent	Reference
Endogenous granules	Human lung fibroblasts	SV80	LTM	22,000	20	<1	0.75	Caspi et al. (2002)
	African green monkey kidney fibroblasts	COS7	LTM	22,000	20	<1	>1	Yamada et al. (2000)
	Mouse macrophage	J774A.1	FLM	60	>5		1	Lau et al. (2003)
	Mouse embryonal carcinoma	F9	FLM	60	>5		1	
	African green monkey kidney epithelial cells	TC7	LTM	50,000	30	<0.001	0.75	Van Citters et al. (2006)
	Bovine aortic endothelial cells	BAEC	LM	20–30	30	>0.02	>1	
	Mouse fibroblasts	L929	LM	1,000	10	>0.7	<1	Dangaria and Butler (2007)
	Human microvascular endothelial cells	Hmec-1	LM	17	150	<0.1	0.5	Rogers et al. (2007)
	Human umbilical vein endothelial cells	HUVEC	LM	20,000	3	>0.5 · 10 ⁻³	0.75	Leijnse et al. (2012)
	Human fetal lung fibroblasts	IMR90	FLM	9	20	>1	0	Li et al. (2009)
Ballistic injection	Mouse fibroblasts	Swiss 3 T3	FLM	30	20	<0.5	<1	Tseng et al. (2002)
	Human umbilical vein endothelial cells	HUVEC-C	FLM	30	20	0.5–10	~1	
	Human microvascular endothelial cells	Hmec-1	LM	17	150	~10	>1	Panorchan et al. (2006)
	Human fetal lung fibroblasts	IMR90	FLM	9	20	<0.3	0	Li et al. (2009)
	Human induced pluripotent stem cells	hiPS				>1	0.92	Daniels et al. (2010)
	Human embryonic stem cells	hES					0 (63 %), 1 (27 %)	
	Mouse fibroblasts	Swiss 3 T3				<0.1	<1	Tseng et al. (2004)
	Human cervix carcinoma epithelial cells	HeLa				0.1–1	0	
	Human cervix carcinoma epithelial cells	HeLa				1–10	>1	Weiss et al. (2004)
	Human cervix carcinoma epithelial cells	HeLa				<0.08	0.51	Guigas et al. (2007)

Table 1 (continued)

Cell type	Designation	Probes ^a	Tracking method	Frame rate (fps)	Total time (s) ^b	Lag time (s)	MSD scaling exponent	Reference
Human hepatocellular epithelial carcinoma	HepG2					<0.08	0.52	
Human liver epithelial cells	THLE					>0.08	1	
						<0.08	0.48	
						>0.08	1	
Natural uptake	SV80	3,000 nm PS lectin	LM	25		<1	1.38–1.56	Caspi et al. (2002)
	TC7	con-A coated 4500 nm magnetic bead coated with RGD	LTM	50,000		>1	0.5–1	
African green monkey kidney epithelial cells						<0.1	~1	Hoffman et al. (2006)
Dicyostelium cells		300, 1,000, 2,800 nm magnetic beads	LM	100		>0.1	>1	
						<4	1.2–1.6	Wilhelm (2008)
Human highly metastatic breast cancer epithelial cells	MDA-MB-231	100 nm CPS	FLM	24	60	<3	1.25	Gal and Weihs (2010)
Human prostatic adenocarcinoma	PC3	Endosomes with 8 nm magnetic beads	LM	60			1.3	Robert et al. (2010)
Human highly metastatic breast cancer epithelial cells	MDA-MB-231	200 nm CPS	FLM	24	60	<6	1.33–1.44	Yizraeli and Weihs (2011)
Primary human fibroblasts						>6	0.78–0.97	
						<0.45	0.78–0.97	
						>0.45	0.97–1.17	
Human highly metastatic breast cancer epithelial cells	MDA-MB-231	200 nm CPS	FLM	60	60	<1	1.4	Gal and Weihs (2012)
Human low metastatic breast cancer epithelial cells	MDA-MB-468					>5	1.06	
Human breast fibrocytic epithelial cells	MCF10A					<1	1.37	
						>5	0.99	
						<1	1.34	
						>5	0.78	

^aProbe diameters (in nanometer) and compositions are provided

^bDenoted time is total measurement time, e.g., video length

CPS carboxylated polystyrene, PS polystyrene, LM light microscopy, LTM laser tracking microscopy, FLM fluorescence microscopy, FCS fluorescence correlation spectroscopy

different approaches on the same cell types in two examples. Hmec-1 cells were evaluated with injected or endogenous particles, differing in particle size and location, yet with the same frame rate and overall time (Li et al. 2009). The observed mechanics were similar yet not identical, as a sub-diffusive exponent appeared at short time scales when particles were injected. Another comparison is available for HeLa cells, where the tracking method was the same, yet the probe particles had different chemistry (Guigas et al. 2007; Weiss et al. 2004). Probe sizes were on the same scale, and observed ranges of MSD scaling exponents were similar. Hence, the experimental design will greatly affect the available and obtained MSD scaling exponents.

Variations between measurements, as observed in Table 1, can also occur due to particle location in the cells. Particle motion near the cell periphery is more hindered as compared to motion at its center and in the nucleus (Leijnse et al. 2012; Li et al. 2009; Tseng et al. 2002). Hence, if particles distribute unevenly or differently inside cells, measurements from dissimilar regions may be compared. Thus, approaches to automatically evaluate the location-dependent motion of the probes within the cells are emerging (Abuhattoum and Weihs 2013). Such approaches require evaluation of the MSD of single particles in the cells.

In summary, in living cells, the MSD is a good first estimator of transport and mechanics, albeit it is not enough to fully characterize this complex intracellular microenvironment or reveal underlying transport mechanisms.

Life after MSD: trajectory and displacement analysis methods

The MSD alone is an insufficient tool for analysis of active systems including living cells. In cells, particle motion is affected by many concurrent active processes. It is typically the active processes together with mechanical responses of cells that are of interest in intracellular studies. However, the MSD cannot reveal underlying mechanisms leading to the observed scaling exponents (Brangwynne et al. 2008; Burov et al. 2011). Moreover, the MSD may conceal transient segments in a trajectory that are averaged out in the calculation (Weihs et al. 2007b). Besides providing misleading data that can generate artifacts and cause misinterpretation, the transient, intermittent nature of the transport is lost. Hence, the limitations of the MSD because of averaging and oversimplification of the transport have instigated development of supplementary analysis tools. Those revisit the particle trajectories with focus on single particles.

Several approaches have been suggested for single-particle trajectory analysis, typically focusing on directionality and displacements as the main parameters. Information

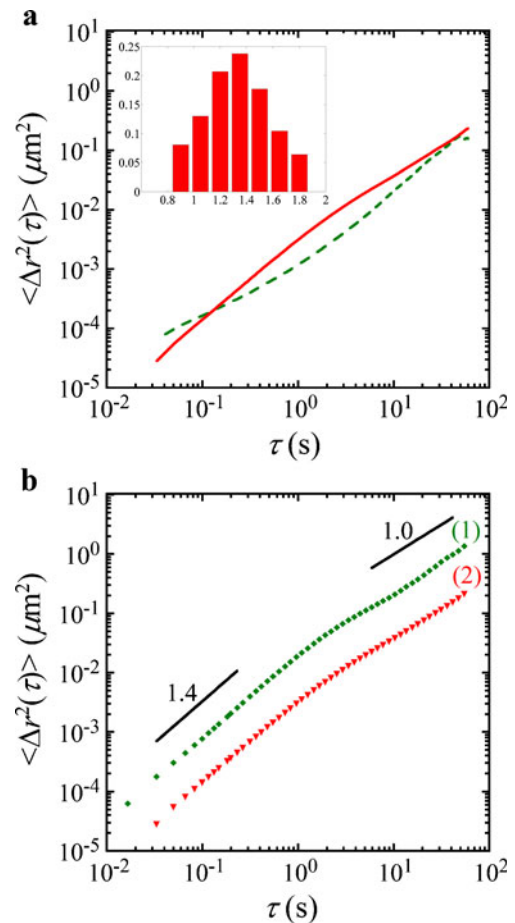


Fig. 1 Time- and ensemble-averaged mean square displacements. **a** MSD of the categorized particles in low MP cells. Most trajectories (92 % of all fit lines) exhibited $\alpha > 0.9$ at short lag times, with $\alpha \sim 1$ at longer lag times (solid line). Few trajectories (8 %) exhibited $\alpha < 0.9$ at short lag times and those had higher α at longer lag times (dashed line). *Inset*: distribution of scaling exponents within the group was continuous and had a single peak. **b** Ensemble-averaged MSD of the large group utilized in subsequent analysis of the (1) high MP cells and the (2) low MP cells. Super-diffusion with $\alpha \sim 1.4$ is observed at short lag times, and scaling exponents reduce at longer lag times. Solid lines are guides to the eye (Gal and Weihs 2012)

obtained from these methods should be combined with input from the MSD. We highlight six different methods in this section that have been applied in particle tracking experiments and demonstrate their utility with sample data from living cells. We illustrate methods that provide (1) the time-dependent directional persistence of trajectories (Raupach et al. 2007); (2) the temporally resolved detection of active regimes (Arcizet et al. 2008); (3) the temporally resolved detection of trapping regimes (Weihs et al. 2012); (4) the trajectory spread in space, calculated through the radius of gyration (Saxton 1993); (5) the Van Hove displacement distributions and deviations from Gaussian

statistics (Valentine et al. 2001); and (6) the self-similarity of a trajectory, using different powers of the displacement (Gal and Weihs 2010). Each presented method reveals different facets of single-particle transport phenomena.

We illustrate each of the methods using data obtained from intracellular particle tracking in living cells. For a full description of the particle tracking experiments and experimental setup, see the paper of Gal and Weihs (2012). We compare low and high metastatic potential (MP) breast cancer cells; the cell lines are MDA-MB-468 and MDA-MB-231, respectively, obtained from the American Tissue Culture Collection. We track intracellular motion of 200 nm diameter, carboxylated polystyrene particles (Molecular Probes-Invitrogen) at a frame rate of 60 fps for 60 s. We only analyze trajectories over 300 frames long (5 s), showing a total about 1,000 particles in more than 100 cells.

Figure 1b shows the ensemble-averaged MSD where the majority of particles in both cells exhibit active motion at short lag times which reduces to sub-diffusive motion at longer lag times. We have only averaged quantitatively and qualitatively similar MSD plots as determined by the MSD scaling exponents for each trajectory; trajectories were obtained using centroid-tracking algorithms (Crocker and Grier 1996; Gal and Weihs 2012) and are available in Gal and Weihs (2012). The MSD scaling exponents were automatically determined for each trajectory using a specialized algorithm (Umansky and Weihs 2012) and were then grouped according to the exponents and the qualitative nature of the motion. The motion of the particles produced two qualitatively different groups, as seen in Fig. 1a. The majority of the particles exhibited exponents of about 1.4 at short lag times which decrease at longer lag times. We utilize the major group of trajectories in the ensuing analyses (Fig. 1b and here on) and provide ensemble averages, where possible, for improved statistics. Using the information gained from the MSD, we proceed to apply each of the methods and discuss their output and contribution to further characterization of the mechanics and dynamics of the cells and differences between them.

Directional persistence

The directionality and directional persistence of a trajectory can provide indication to mechanisms driving the particle motion. This approach has shown that the constant remodeling in a tensed cytoskeleton drives spontaneous motion of particles attached to the cytoskeleton through the cell membrane (Raupach et al. 2007); it can also be applied to intracellular particle motion.

The method entails determination of time-dependent directional changes in the trajectory. The directional chan-

ges are evaluated by a turning angle between each set of three points on the trajectory. The points are defined by window of specified duration that is moved on the length of the trajectory. By sliding the window along the trajectory, the distribution of turning angles for a particle is obtained as a function of lag time (Berg and Brown 1972). The distribution of turning angles indicates relative incidence of random, persistently directional, or anti-persistent motion of the particles. For random motion, successive turning angles are independent and can exhibit any value in the range $[-\pi, \pi]$ with equal probability in each time window. Conversely, for persistent or anti-persistent motion, the directionality is, respectively, correlated or anti-correlated between successive time intervals. That results in more obtained angles around zero for persistent, directed motions, or close to $\pm\pi$ for anti-persistent motions. To combine information from the turning angles, an index of directionality, P_d , is defined as the difference between the probabilities of forward and backward motions. A P_d of zero indicates random motion, while positive or negative values, respectively, signify persistent and anti-persistent motions. To detect time-dependent processes, the P_d is evaluated as a function of lag time. For example, consistent increase in P_d with lag time indicates that the directionality becomes increasingly dominant. Directional persistence can indicate local flow or drift or existence of ballistic, active transport. Active motion driven by motors may, however, not be ballistic, directional, or directionally persistent (Kahana et al. 2008); thus, it is important to also consider the MSD and the trajectory when suggesting a mechanism. In contrast, anti-persistent motion may be caused by elasticity of the medium (local trapping) or by motor switching, inducing rapid changes in direction when observed at characteristic lag times (Kahana et al. 2008). We have calculated the time-dependent directional persistence for each particle and then ensemble-averaged the P_d for all the particles.

Figure 2 shows that particle trajectories are markedly more directional and directionally persistent in the low MP cells. The low MP cells exhibited anti-persistent motion at short lag times and transitioned to highly persistent motion above 0.1 s. That could indicate confined short time-scale steps superimposed on directional motion, which becomes more dominant at longer lag times, as apparent by the consistent change in slope. This corresponds to observed trajectories (Gal and Weihs 2012) and could suggest active transport along a filament, for example, by molecular motors. In contrast to the low MP cells, the high MP cells were initially non-directional and became directionally persistent, albeit exhibiting a maximum at about 0.3 s. This could indicate that directional persistence cannot be maintained for prolonged periods of time in the high MP cells. In both cells, the persistent directionality

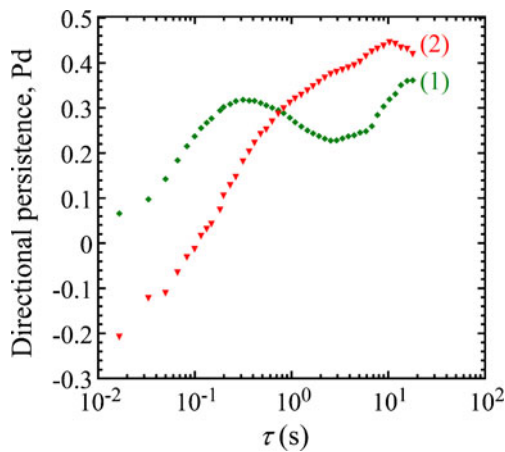


Fig. 2 Persistent directionality in ensembles of all the particles in the (1) high MP cells and (2) low MP cells (Gal and Weihs 2012)

corresponds with active transport regimes as determined from the MSD. At longer lag times (5–10 s), we observe changes in MSD scaling exponents that are also reflected in the Pd of both cell types. Note that despite being more directionally persistent, the overall distance covered by particles in the low MP cells remains small with respect to the high MP cells as is apparent through the difference in amplitudes of the MSD (Fig. 1b). That is likely due to the dense cytoskeletal network in the low MP cells (Gal and Weihs 2012) and underscores the importance of revisiting the MSD following each analysis approach.

Temporally resolved detection of convective regimes

A similar approach, yet with different focus, is to simultaneously evaluate directionality together with convective motion, as indicated by the MSD scaling exponents. That approach is designed to detect segments of simultaneously directional and nearly ballistic motion typically associated with molecular motor transport (Arcizet et al. 2008).

In this method, a measure of the directional persistence is determined for sliding time windows and is combined with the MSD scaling exponent in each window. The local time-dependent MSD is calculated within sliding user-defined windows of M frames and then fit to a power law to obtain the local MSD scaling exponent, α . Concurrently, an angle correlation function in the range $[-\pi, \pi]$ is calculated through the same windows, providing the directional persistence in that window. Directionality is defined when the absolute value of the angle is under 0.6, where for unidirectional motion the angle correlation function is zero. The critical angle correlation function is given a limit above zero to include slow directional changes in the underlying cytoskeletal tracks (Arcizet et al. 2012). In parallel with directionality determination in the window, the MSD scaling exponent is used to identify convection. Convective

motion is defined in this method when the MSD scaling exponent is >1.7 ; this cutoff is chosen to include strictly active motion. When the defined conditions for the local MSD scaling and the angle correlation function occur simultaneously, a convective regime is defined. The convective regime determined here is assumed to result from molecular motor-mediated transport (Arcizet et al. 2008). It is important to note that motor-mediated convection can also be non-directional (Kahana et al. 2008; Snider et al. 2004) and will not be detected with this approach. Following detection of convective regimes, it is possible to evaluate their frequency of appearance and temporal persistence.

Figure 3 shows that the detected convective segments are of similar length in both cells. The low MP cells exhibited convective segments in about half as many particles as the high MP cells at all chosen window sizes (data not shown). As window size was increased, fewer particles were

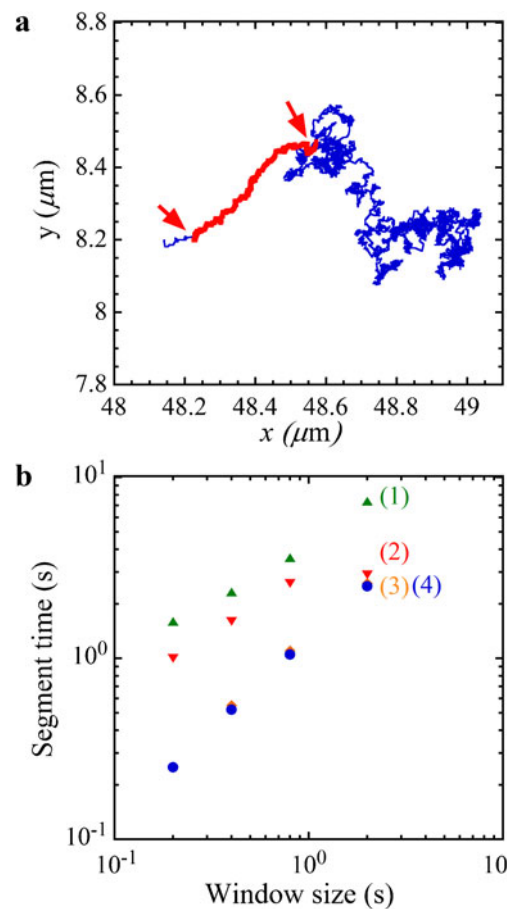


Fig. 3 Detected convective segments in trajectories. **a** Representative single trajectory with detected convective segment marked with arrows. **b** Average convective or non-convective segments lengths in (1, up-pointing triangle) non-convective segment in low MP cells; (2, down-pointing triangle) non-convective segment in high MP cells; (3, diamond) convective segment in high MP cells are overlapped by (4, circle) convective segment in low MP cells

detected as convective in both cells, but segments became longer. Convective segment lengths in both cells were the same for all windows. In contrast, the lengths of the non-convective segments that connect convective segments were longer in the low MP cells as compared to the high MP cells. When the chosen time windows are very short, the statistics for accurate calculation of the local MSD scaling exponent are insufficient, and the algorithm may also erroneously detect non-convective regions as convective; e.g., short regions within a simulated, purely diffusive trajectory have been identified as convective with very short windows (data not shown). It is, thus, advisable to choose windows that are typically no less than 1 s long and rely on motions identified through MSD scaling exponents that persist for at least half a time decade.

Temporally resolved detection of trapping regimes

An inherently different approach for detecting intermittent trapping regimes is to scan the entire trajectory for the “aftermath” of a local confinement—a dense region of many overlapping steps (Weihs et al. 2012). That allows easy detection of traps, which only become apparent after prolonged periods of time, when a moving particle has repeatedly encountered the trap edges (Weihs et al. 2007b); smaller traps are apparent in less time/steps.

The method requires consideration of the entire trajectory as an image, initially without regard for time, to detect regions with large step density. A particle within an elastic confinement on the same scale as its radius will exhibit many back-and-forth steps. This will produce a dense region in the image of the trajectory that can be detected with an appropriately chosen density threshold. The choice of the threshold is critical in this method and has been designed to be done automatically. Automatic choice of the threshold is performed using a preconditioned algorithm that has been optimized for a wide range of experimental parameters. The parameters affecting the threshold include the particle size, relative size of the confinement, the confinement time, and the experimental setup; e.g., camera frame rate. Using simulated trajectories with a wide range of system and experiment parameters (Weihs et al. 2007b), the threshold was preconditioned for optimal detection. Optimal thresholds are, thus, automatically calculated following user selection of cutoffs for the minimal confinement time and the size ratio of particle to trap; those indicate what a user would like to define as a trap. Following threshold application and trap detection, the time dependence of the trajectory steps is reintroduced. The sequence order of steps is known, and thus, segment continuity may be verified and the mode of motion, confirmed by the segment’s MSD. The MSD of even a short trajectory segment in a trap will plateau ($\alpha = 0$), where the plateau is proportional to the

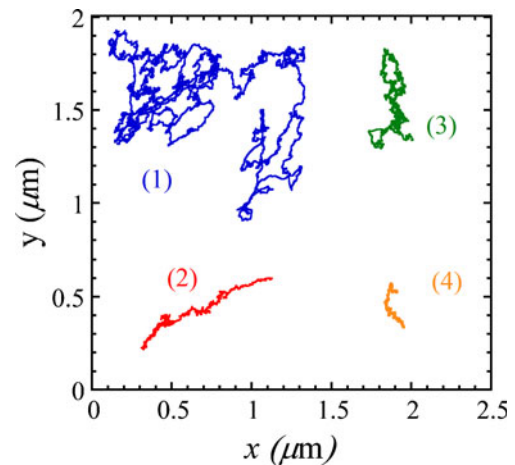


Fig. 4 Representative trajectories observed in the high and low MP cells. No trapping segments were detected in any trajectory in either cell type even when particles appeared to linger in regions. (1, 2) high MP cells (3, 4) low MP cells

trap size (Tseng et al. 2004; Weihs et al. 2007b). Conversely, a diffusive trajectory of a particle randomly sampling its immediate region will exhibit no MSD plateau. Hence, the MSD and the MSD scaling exponents can be used to filter out any clearly diffusive regimes that may have been incorrectly detected. The MSD may, however, exhibit small scaling exponents (close to a plateau) due to viscoelasticity of the medium or less likely due to vertical motion that is tracked in 2D; vertical motion would have to persist for long times for this to be identified. Thus, absolutely detecting traps may be difficult, yet regions of local motion inhibition can be identified.

Figure 4 shows that in the two cell lines evaluated here, no intermittent trap–escape trajectories were detected exist. Such trajectories typically occur when there is structural obstruction to particle motion, e.g., when the microenvironment structure includes effective cages. Caged particles will exhibit confinement together with intermittent escape segments (active or diffusive). Escape is facilitated through cage-structure dynamics or when a particle gains sufficient energy to jump out of the cage. Many very different systems have exhibited intermittent particle diffusion in cages. Those include complex materials (Weeks et al. 2000), interiors of yeast cells (Golding and Cox 2006; Jeon et al. 2011; Weber et al. 2010), interiors of living mammalian cells (Bronstein et al. 2009; Suh et al. 2004), and membrane regions of mammalian cells (Bursac et al. 2005).

Trajectory spread in space—radius of gyration

The distance that a particle travels in a given time depends on the forces driving its motion and the traversed microenvironment. Hence, differences in activity and mechanics of

two samples can be evaluated by comparing the traveled distance away from the start or the spread of the trajectories in those regions (Saxton 1993).

The amount of spread of a trajectory can be evaluated with the radius of gyration (R_g), or other measures of distances at a given time; the R_g has typically been used to determine the size of a polymer chain (Rubinstein and Colby 2003). Here, the R_g is defined as the root mean square distance between each time-dependent step and the center of mass. For a trajectory with a total of N frames, the R_g is given by $R_g^2 = \frac{1}{N} \sum_{i=1}^N (\vec{R}_i - \vec{R}_{cm})^2$,

where \vec{R}_i and \vec{R}_{cm} are, respectively, the particle location at frame- i and the trajectory's center of mass (Rubinstein and Colby 2003). The R_g can also be calculated as the average of the distances between all measured positions in a trajectory:

$$R_g^2 = \frac{1}{2N^2} \sum_{i=1}^N \sum_{j=i}^N (\vec{R}_i - \vec{R}_j)^2.$$

Hence, the R_g simultaneously takes into account all time-scales providing an averaged measure of the trajectory size. Note that with the effective normalization by trajectory length (N), the R_g from trajectories with different lengths can be compared on the same plot. An inherent assumption of the R_g calculation is that each sequential step is statistically independent, which is not the case for motion in a viscoelastic medium; hence, we also present for comparison a similar magnitude that does not require this assumption. The time scale of sampling determines what is estimated by the R_g . At long times, longer than any relaxation time (memory) of the material, the sequential steps become independent, and we obtain a measure for the diffusion coefficient of the particle as $\sim R_g^2/\tau$. For shorter times, we simply obtain a comparative measure of the developing trajectories.

Figure 5 shows the cumulative distribution functions of the trajectory spreading in the high and low MP cells using three different measures. We have initially calculated the radius of gyration of particle trajectories (Fig. 5a), as detailed above. For comparison, we have also determined the distance traveled by particles after 10 s from their initial detection and the value of the MSD at $\tau = 10$ s (Fig. 5b, c). Those measures simply show the absolute and average traveled distance, respectively, at a given time; the former does not assume independence of the steps. All three approaches showed qualitatively similar results: a log-normal distribution of particle displacements in both cells, with lower values in the low MP cells. The spread of trajectories in the low MP cells were significantly smaller than those of the high MP cells. This indicates that particles move farther in the high MP cells, which again correlates with the higher MSD amplitude in Fig. 1. The ability of particles to move more in the high MP cells is likely because, concurrently, their intracellular environment is less dense and more

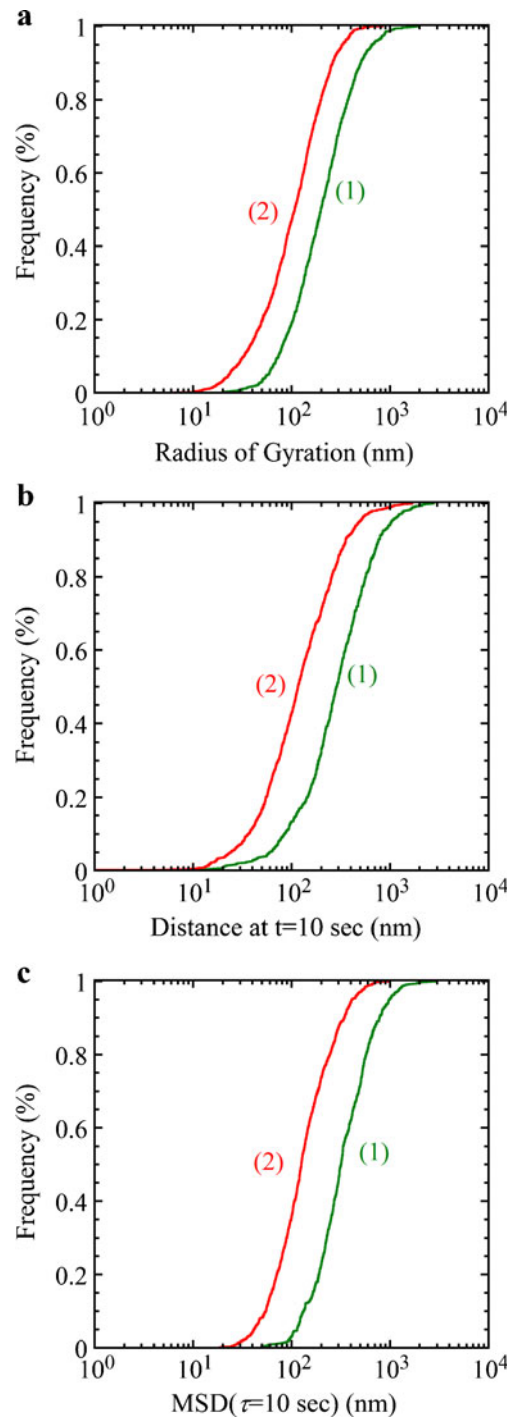


Fig. 5 Cumulative distribution functions of the high MP (1) and low MP (2) cells, by calculation of the **a** radius of gyration, **b** distance traveled after $t = 10$ s, and **c** MSD ($\tau = 10$ s)

active than that of the low MP cells. The R_g and the distance measures provide tools to compare trajectories in different systems.

Van Hove displacement distributions and deviations from Gaussian statistics

The time-dependent probability distributions of the observed displacements and their deviation from Gaussian statistics can reveal existence of active modes of motion (Valentine et al. 2001). Motions that are driven by active transport will deviate from a Gaussian distribution. That deviation has been quantified using two different non-dimensional parameters (Rich et al. 2011; Weeks et al. 2000).

The approach dictates plotting the displacement distributions at lag times of interest and evaluating their deviation from Gaussian statistics. The one-dimensional displacements $\Delta x(\tau) = x(t + \tau) - x(t)$ at a lag time τ can be collected into a probability distribution plot $P(\Delta x, \tau)$ for each particle or for the ensemble. The probability distribution of the particle displacements is known as the ensemble-averaged van Hove correlation function (Van Hove 1954). The van Hove correlation function of Brownian thermally driven particles will simply be a single Gaussian distribution. In contrast, displacements driven by active intracellular processes will deviate from the Gaussian distribution. The deviation from the Gaussian can be emphasized by plotting the ratio of the widths of Gaussian fits to the ensemble-averaged van Hove correlations (Stuhrmann et al. 2012).

The deviation from the Gaussian behavior can be quantified by the time-dependent non-Gaussian parameter (NGP): $\alpha_2(\tau) = \frac{\langle \Delta x^4(\tau) \rangle}{3\langle \Delta x^2(\tau) \rangle^2} - 1$, where the $\langle \Delta x^k(\tau) \rangle = \frac{1}{N} \sum_i x_i^k(\tau)$ are estimators for the k th moments of the distribution (Rahman 1964; Weeks et al. 2000). The NGP is, in fact, the kurtosis of the displacements Δx . For a pure Gaussian distribution, the NGP is $\alpha_2 = 0$, while for non-Gaussian distributions the α_2 will not vanish. Although a non-zero α_2 reveals deviations from Gaussian statistics, its specific value is irrelevant and provides no indication to the mechanisms driving the motion. Recently, the heterogeneity ratio $HR = M_2(\tau)/M_1^2(\tau)$ had been suggested as an equivalent yet improved measure of deviation from Gaussian statistics (Rich et al. 2011). The M_1 and M_2 are the weighted ensemble-averaged MSD and weighted ensemble-averaged variance of the MSD, respectively. The weighting takes into account differences in trajectory lengths, reducing statistical bias. However, if the NGP is calculated directly from the raw data, it will inherently be weighted, as all the displacements are taken into account and shorter trajectories will contribute fewer Δx 's.

Figure 6 shows that displacements in both cell types are non-Gaussian, and the deviations correlate with time scales observed in the MSD. Both cell types exhibit displacement distributions with a Gaussian center, yet with so-called

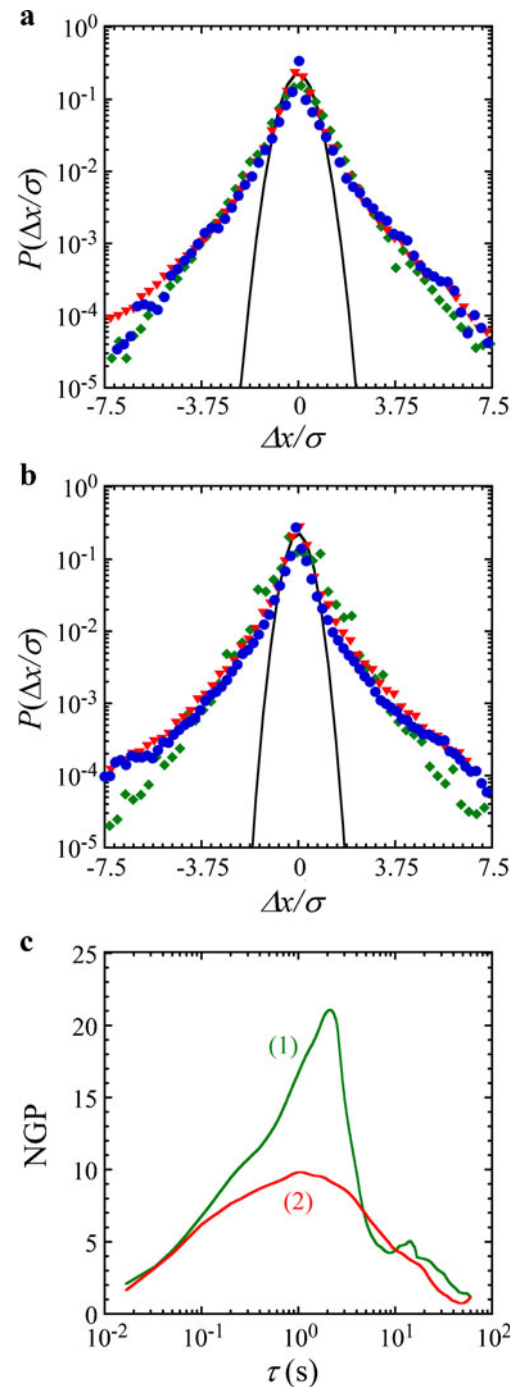


Fig. 6 The van Hove correlation function and non-Gaussian parameter in both cell types. van Hove correlation function at lag times of $\tau = 0.0167$ s (diamond), $\tau = 0.5$ s (down-pointing triangle), and $\tau = 5$ s (circle) for the **a** high MP cells and **b** low MP cells. The displacement distributions were normalized by their respective standard deviations for clarity. The *solid line* is a single Gaussian distribution. **c** Time-dependent non-Gaussian parameter for (1) high MP cells and (2) low MP cells

“heavy tails” that are distinctly higher than the Gaussian. In parallel, the NGP also shows existence of non-thermal, likely active driving processes. The α_2 increase to maxima

in the midrange time scales and vanish at short and long lag times (Fig. 6c). Similar $\alpha_2(\tau)$ plots have been attributed to small non-thermal driving forces (Toyota et al. 2011), which are likely in the dense intracellular microenvironment. The non-thermal forces that induce the increase in the NGP also affect the form of the MSD. Thus, the maxima in the α_2 occur at the same times as the crossover from super-diffusive to diffusive-like scaling in the ensemble-averaged MSD (Fig. 1). At the shortest and longest times, the NGP is expected to vanish (Rahman 1964), as observed here, albeit for different reasons. The NGP vanishes at the shortest lag times, as the underlying thermally driven motion is dominant and induces a Gaussian distribution of the steps. A random distribution is again obtained at long lag times, due to motor switching between filaments resulting in an effective random motion (Kahana et al. 2008; Snider et al. 2004). The NGP provides a relative measure to compare the two cell types. However, it is unclear from this parameter if variations result from different driving mechanisms (forces) or structural environments, which also affect the MSD amplitude.

Self-similarity of a trajectory

Existence of different and concurrent active transport processes can be revealed through deviations of trajectories from self-similarity (Gal and Weihs 2010). Self-similar trajectories exhibit scale invariance, which occurs when all steps belong to the same apparent distribution (e.g. in diffusion). Conversely, two or more step distributions may coincide when concurrent, thermal and various active driving mechanisms coexist, causing weakly self-similar motions.

In this method, the time-dependent displacements are raised to a range of powers other than the second (i.e., the MSD) and the power dependence of the scaling exponents is evaluated for a specific range of lag times. The powers q of the displacements induce a time-dependent response proportional to the power $\langle \Delta r^q(\tau) \rangle = \langle |\Delta r(t+\tau) - \Delta r(t)|^q \rangle \sim \tau^{qv(q)}$, where the scaling exponents $qv(q)$ provide a measure for the self-similarity of a trajectory (Castiglione et al. 1999; Ferrari et al. 2001). A trajectory producing a set of Gaussian-distributed displacements will be strongly self-similar and, thus, scale invariant. That is, the trajectory will appear the same on any time scale, and displacement exponents $qv(q)$ will be linear with the power q with a slope $v(q) = 0.5$ at all powers; an algorithm has recently been suggested to validate the specific case of (sub-diffusive) fractional Brownian motion where trajectories are stationary, Gaussian, ergodic, and exhibit mixing (Burneck et al. 2012). The slope of the scaling exponents provides a basic indication of transport mechanisms. Actively driven displacements will exhibit $0.5 < v(q) \leq 1$ up to purely convective ballistic motion

(if $v(2) = 1$, then $\alpha = 2$), where the scaling exponents remain linear; similar to the MSD, this approach cannot directly reveal what is the active mechanism. Non-linearity of the scaling exponents, or a non-constant $v(q)$, indicate further deviation from Gaussian and existence of other mechanisms driving or resisting motion. Of particular interest are weakly self-similar trajectories which are defined by a piecewise bilinear $qv(q)$, with two non-decreasing slopes, and $v(2) > 0.5$, (Andersen et al. 2000; Castiglione et al. 1999; Ferrari et al. 2001; Leoncini et al. 2004; Pikovsky 1991). The last condition translates to an MSD scaling exponent $\alpha > 1$ that indicates active motion. However, this is not simple active transport, as the bilinear form indicates a weakly self-similar trajectory, which likely results from at least two concurrent active mechanisms driving the motion.

Figure 7 shows that particle motion in both low MP and high MP cells is actively driven, yet the resulting trajectories exhibit strong and weak self-similarity, respectively. The scaling exponents were obtained in the range of 0.1–1 s for all powers of the displacements, where the MSD indicated active transport. The low MP cells exhibit a single slope $v(q) = 0.65$, indicating super-diffusive yet sub-ballistic motion. In contrast, in the high MP cells, we observe a bilinear scaling which indicates weak self-similarity. The initial slope of the scaling exponents in the high MP cells matches that observed in the low MP cells ($v(q \leq 2) = 0.65$). However, a second slope $v(q \geq 2) = 0.85$ emerges at large q . That second slope results from rarely appearing large displacements, about 2 % of all steps (Gal and Weihs 2010). While those steps are averaged out at small powers of the displacement, they are accentuated at larger powers. Hence, the weakly self-similar motion in the high MP cells could

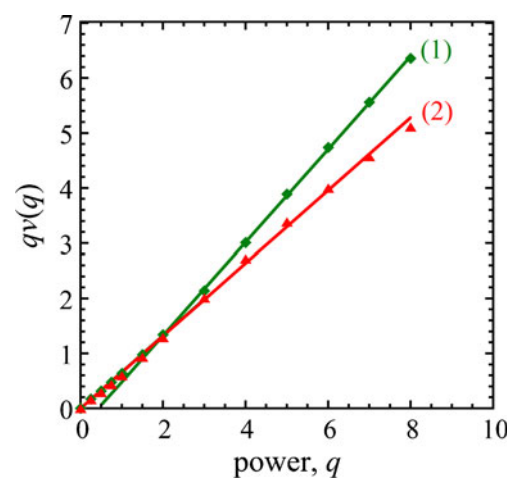


Fig. 7 Scaling exponents of the displacements at each power, q , in the (1) high MP, and (2) low MP cells. At low moment orders $q \leq 2$, a slope of ~ 0.65 was observed in both cell lines. At higher moment orders $q \geq 2$, a second slope of 0.85 was observed in high MP cells alone (Gal and Weihs 2012)

result from intermittent segments of highly active transport in an inherently active trajectory. Those may relate to the high-frequency ballistic regimes predicted and observed in cells following rapid decay of built-up stress in the cells (Head and Mizuno 2010). It is important to note that those rare, highly active steps are not necessarily sequential and, thus, may not be detected with sliding window approaches.

Summary

In the past decade, a large variety of intracellular particle tracking experiments have been carried out, where the MSD and its scaling exponents have served as the main analysis tools. Table 1 shows the interesting collection of results, with clear similarities and differences. It is apparent that the measurements depend greatly on the experimental setup. Specifically, the frame rate, particle size, and its location, which are partially determined by internalization technique, affect the measured MSD and its scaling exponents. We do observe a general difference between particle transport deep within living cells and that measured following injection (typically to the cell cortex) or by endogenous particles. Hence, particle internalization and localization strongly affect particle transport, as is revealed through the MSD. However, as informative as the MSD is, it is still limited in what it can provide.

The methods presented here to augment the MSD revealed several more levels of information available in the raw particle tracking data—particle trajectories in the living cells. Through various the trajectory- and displacement-based approaches, we have observed differences between high and low MP cells that were not apparent in the MSD. The ensemble MSD showed a difference between the two cell types only in the MSD amplitudes, yet exhibited similar MSD scaling exponents and transition times. In contrast, the analysis methods beyond the MSD have revealed many more differences that can help to converge on the nature of active transport processes in the cells. We have observed both directional and convective segments in both cell types, albeit with different characteristics and rates of recurrence. We have also observed a relation between the deviation of displacements from Gaussian distribution and the time scales observed in the MSD. Moreover, in evaluating powers other than the second, we were able to show existence of rare, highly active events in the high MP cells that do not exist in the low MP cells. We deduce that particles in the cells mostly experience small non-thermal forces, which induce steps on the order of thermally mediated displacements. Those non-thermal forces likely result from direct or indirect interactions with molecular motors in the cells and, in the high MP cells, are at times augmented by a different

process. Hence, the methods and algorithms described here indirectly suggest mechanisms driving particle motion.

We suggest usage and interpretations that can be reached using each of the described methods. Each method reveals an element of the observed motion and can be used to construct a hypothesis regarding intracellular structure and transport mechanisms; some of the methods are only comparative, such as the R_g and the NGP. For example, if local trapping or a small R_g are observed, that could indicate dense and/or stiff intracellular structures. Similarly, existence of segments of convective or directional motion will typically relate to the local structure and driving element, while non-directional activity could also result from remodeling of the cytoskeleton; segments can be analyzed as parts of trajectories if they are long enough. Non-directional active transport will not be revealed by directionality- and persistence-based analyses approaches but will require comparisons of displacements. The displacements can reveal deviation from Gaussian distribution and also existence of more than one active driving process. Not all the methods will be relevant to every experimental data set and may provide negative answers (as illustrated here for intermittent trapping). However, even a negative result from a specific method can provide indication to the driving mechanisms and local structure. It is important to keep in mind that a single method will typically not provide conclusive proof of the transport mechanisms or structure and rheology of the probed microenvironment. Hence, careful analysis is required to prove that what is observed arises from a specifically suggested mechanism. For validation, results from several analysis methods can be correlated and also combined with particle tracking experiments under specifically targeted drug-induced disruptions to the cells; e.g., disruption of motor function can help confirm motor transport. In conclusion, the introduced methods for advanced particle tracking analysis provide a much more in-depth view of particle transport in cells than available from the MSD alone. The MSD and other approaches have revealed many interesting aspects of intracellular mechanics and transport in the last decades. However, while particle tracking measurements have been performed on many cell types, a more systematic approach is required. We believe that the approaches highlighted herein are essential for any significant progress in understating the mechanisms driving particle transport and through them, mechanisms and structure of cells in general.

Acknowledgments The authors thank Rony Granek for the stimulating discussions. The work was partially funded by the Israeli Ministry of Science and Technology and the Eliyahu Pen Fund for Scientific and Medical Research.

References

- Abuhattoum S, Weihs D (2013) Location-dependent intracellular particle tracking using a cell-based coordinate system. *Comput Methods Biomech Biomed Eng*. doi:[10.1080/10255842.2012.761694](https://doi.org/10.1080/10255842.2012.761694)
- Andersen KH, Castiglione P, Mazzino A, Vulpiani A (2000) Simple stochastic models showing strong anomalous diffusion. *Eur Phys J B* 18:447–452
- Arcizet D, Capito S, Gorelashvili M, Leonhardt C, Vollmer M, Youssef S, Rappl S, Heinrich D (2012) Contact-controlled amoeboid motility induces dynamic cell trapping in 3D-microstructured surfaces. *Soft Matter* 8:1473–1481. doi:[10.1039/C1sm05615h](https://doi.org/10.1039/C1sm05615h)
- Arcizet D, Meier B, Sackmann E, Radler JO, Heinrich D (2008) Temporal analysis of active and passive transport in living cells. *Phys Rev Lett* 101. doi:[10.1103/PhysRevLett.101.248103](https://doi.org/10.1103/PhysRevLett.101.248103)
- Asnacios A, Desprat N, Guiroy A (2006) Microplates-based rheometer for a single living cell. *Rev Sci Instrum* 77. doi:[10.1063/1.2202921](https://doi.org/10.1063/1.2202921)
- Bao G, Suresh S (2003) Cell and molecular mechanics of biological materials. *Nat Mater* 2:715–725. doi:[10.1038/Nmat1001](https://doi.org/10.1038/Nmat1001)
- Bausch AR, Ziemann F, Boulbitch AA, Jacobson K, Sackmann E (1998) Local measurements of viscoelastic parameters of adherent cell surfaces by magnetic bead microrheometry. *Biophys J* 75:2038–2049
- Berg HC, Brown DA (1972) Chemotaxis in *Escherichia coli* analysed by three-dimensional tracking. *Nature* 239:500–504
- Binnig G, Quate CF, Gerber C (1986) Atomic force microscope. *Phys Rev Lett* 56:930–933
- Brangwynne CP, Koenderink GH, MacKintosh FC, Weitz DA (2008) Nonequilibrium microtubule fluctuations in a model cytoskeleton. *Phys Rev Lett* 100. doi:[10.1103/PhysRevLett.100.118104](https://doi.org/10.1103/PhysRevLett.100.118104)
- Brangwynne CP, Koenderink GH, Weitz DA, MacKintosh FC (2009) Intracellular transport by active diffusion. *Trends Cell Biol* 19:423–427. doi:[10.1016/j.tcb.2009.04.004](https://doi.org/10.1016/j.tcb.2009.04.004)
- Bronstein I, Israel Y, Kepten E, Mai S, Shav-Tal Y, Barkai E, Garini Y (2009) Transient anomalous diffusion of telomeres in the nucleus of mammalian cells. *Phys Rev Lett* 103:018102. doi:[10.1103/PhysRevLett.103.018102](https://doi.org/10.1103/PhysRevLett.103.018102)
- Brown R (1828) On the particles contained in the pollen of plants and on the general existence of active molecules in organic and inorganic bodies. *Edinburgh New Phil J*:358–371
- Burnecki K, Kepten E, Janczura J, Bronshtein I, Garini Y, Weron A (2012) Universal algorithm for identification of fractional Brownian motion. A case of Telomere subdiffusion. *Biophys J* 103:1839–1847. doi:[10.1016/j.bpj.2012.09.040](https://doi.org/10.1016/j.bpj.2012.09.040)
- Burov S, Jeon JH, Metzler R, Barkai E (2011) Single particle tracking in systems showing anomalous diffusion: the role of weak ergodicity breaking. *Phys Chem Chem Phys* 13:1800–1812. doi:[10.1039/C0cp01879a](https://doi.org/10.1039/C0cp01879a)
- Bursac P, Lenormand G, Fabry B, Oliver M, Weitz DA, Viasnoff V, Butler JP, Fredberg JJ (2005) Cytoskeletal remodelling and slow dynamics in the living cell. *Nat Mater* 4:557–561. doi:[10.1038/Nmat1404](https://doi.org/10.1038/Nmat1404)
- Cameron AR, Frith JE, Cooper-White JJ (2011) The influence of substrate creep on mesenchymal stem cell behaviour and phenotype. *Biomaterials* 32:5979–5993. doi:[10.1016/j.biomaterials.2011.04.003](https://doi.org/10.1016/j.biomaterials.2011.04.003)
- Caspi A, Granek R, Elbaum M (2000) Enhanced diffusion in active intracellular transport. *Phys Rev Lett* 85:5655–5658
- Caspi A, Granek R, Elbaum M (2002) Diffusion and directed motion in cellular transport. *Phys Rev E Stat Nonlinear Soft Matter Phys* 66:011916
- Castiglione P, Mazzino A, Muratore-Ginanneschi P, Vulpiani A (1999) On strong anomalous diffusion. *Physica D* 134:75–93
- Chaudhuri O, Parekh SH, Lam WA, Fletcher DA (2009) Combined atomic force microscopy and side-view optical imaging for mechanical studies of cells. *Nat Methods* 6:383–U392. doi:[10.1038/Nmeth.1320](https://doi.org/10.1038/Nmeth.1320)
- Cheezum MK, Walker WF, Guilford WH (2001) Quantitative comparison of algorithms for tracking single fluorescent particles. *Biophys J* 81:2378–2388
- Chen DTN, Wen Q, Janmey PA, Crocker JC, Yodh AG (2010) Rheology of soft materials. *Ann Rev Cond Mat Phys* 1:301–322. doi:[10.1146/annurev-conmatphys-070909-104120](https://doi.org/10.1146/annurev-conmatphys-070909-104120)
- Crick FHC, Hughes AFW (1950) The physical properties of cytoplasm—a study by means of the magnetic particle method .I. Experimental. *Exp Cell Res* 1:37–80. doi:[10.1016/0014-4827\(50\)90048-6](https://doi.org/10.1016/0014-4827(50)90048-6)
- Crocker JC, Grier DG (1996) Methods of digital video microscopy for colloidal studies. *J Colloid Interface Sci* 179:298–310
- Crocker JC, Hoffman BD (2007) Multiple-particle tracking and two-point microrheology in cells. *Methods Cell Biol* 83:141–178. doi:[10.1016/S0091-679X\(07\)83007-X](https://doi.org/10.1016/S0091-679X(07)83007-X)
- Crocker JC, Valentine MT, Weeks ER, Gisler T, Kaplan PD, Yodh AG, Weitz DA (2000) Two-point microrheology of inhomogeneous soft materials. *Phys Rev Lett* 85:888–891
- Cross SE, Jin YS, Rao J, Gimzewski JK (2007) Nanomechanical analysis of cells from cancer patients. *Nat Nanotechnol* 2:780–783. doi:[10.1038/nnano.2007.388](https://doi.org/10.1038/nnano.2007.388)
- Dangaria JH, Butler PJ (2007) Macrorheology and adaptive microrheology of endothelial cells subjected to fluid shear stress. *Am J Physiol Cell Physiol* 293:C1568–C1575. doi:[10.1152/ajp-cell.00193.2007](https://doi.org/10.1152/ajp-cell.00193.2007)
- Daniels BR, Hale CM, Khatau SB, Kusuma S, Dobrowsky TM, Gerecht S, Wirtz D (2010) Differences in the microrheology of human embryonic stem cells and human induced pluripotent stem cells. *Biophys J* 99:3563–3570. doi:[10.1016/j.bpj.2010.10.007](https://doi.org/10.1016/j.bpj.2010.10.007)
- Dasgupta BR, Tee SY, Crocker JC, Frisken BJ, Weitz DA (2002) Microrheology of polyethylene oxide using diffusing wave spectroscopy and single scattering. *Phys Rev E* 65. doi:[10.1103/PhysRevE.65.051505](https://doi.org/10.1103/PhysRevE.65.051505)
- de Vries AHB, Krenn BE, van Driel R, Kanger JS (2005) Micro magnetic tweezers for nanomanipulation inside live cells. *Biophys J* 88:2137–2144. doi:[10.1529/biophysj.104.052035](https://doi.org/10.1529/biophysj.104.052035)
- Discher D, Dong C, Fredberg JJ, Guilak F, Ingber D, Janmey P, Kamm RD, Schmid-Schonbein GW, Weinbaum S (2009) Biomechanics: Cell research and applications for the next decade. *Ann Biomed Eng* 37:847–859. doi:[10.1007/s10439-009-9661-x](https://doi.org/10.1007/s10439-009-9661-x)
- Discher DE, Janmey P, Wang YL (2005) Tissue cells feel and respond to the stiffness of their substrate. *Science* 310:1139–1143. doi:[10.1126/science.1116995](https://doi.org/10.1126/science.1116995)
- Einstein A (1905) On the movement of small particles suspended in a stationary liquid demanded by the molecular-kinetic theory of heat. *Annalen der Physik (Leipzig)* 17:549–560
- Engler AJ, Sen S, Sweeney HL, Discher DE (2006) Matrix elasticity directs stem cell lineage specification. *Cell* 126:677–689. doi:[10.1016/j.cell.2006.06.044](https://doi.org/10.1016/j.cell.2006.06.044)
- Evans E, Ritchie K, Merkel R (1995) Sensitive force technique to probe molecular adhesion and structural linkages at biological interfaces. *Biophys J* 68:2580–2587
- Fabry B, Maksym GN, Butler JP, Glogauer M, Navajas D, Fredberg JJ (2001) Scaling the microrheology of living cells. *Phys Rev Lett* 87. doi:[10.1103/PhysRevLett.87.148102](https://doi.org/10.1103/PhysRevLett.87.148102)
- Ferrari R, Manfroi AJ, Young WR (2001) Strongly and weakly self-similar diffusion. *Physica D* 154:111–137
- Fletcher DA, Mullins D (2010) Cell mechanics and the cytoskeleton. *Nature* 463:485–492

- Freundlich H, Seifriz W (1923) On the elasticity of soles and gels. *Z Phys Chem-Stoch Ve* 104:233–261
- Gal N, Weihs D (2010) Experimental evidence of strong anomalous diffusion in living cells. *Phys Rev E* 81:020903(R). doi:[10.1103/PhysRevE.81.020903](https://doi.org/10.1103/PhysRevE.81.020903)
- Gal N, Weihs D (2012) Intracellular mechanics and activity of breast cancer cells correlate with metastatic potential. *Cell Biochem Biophys* 63:199–209. doi:[10.1007/s12013-012-9356-z](https://doi.org/10.1007/s12013-012-9356-z)
- Gallet F, Arcizet D, Bohec P, Richert A (2009) Power spectrum of out-of-equilibrium forces in living cells: amplitude and frequency dependence. *Soft Matter* 5:2947–2953. doi:[10.1039/B901311c](https://doi.org/10.1039/B901311c)
- Gittes F, Schnurr B, Olmsted PD, MacKintosh FC, Schmidt CF (1997) Microscopic viscoelasticity: shear moduli of soft materials determined from thermal fluctuations. *Phys Rev Lett* 79:3286–3289
- Golding I, Cox EC (2006) Physical nature of bacterial cytoplasm. *Phys Rev Lett* 96:098102. doi:[10.1103/PhysRevLett.96.098102](https://doi.org/10.1103/PhysRevLett.96.098102)
- Granek R (1997) From semi-flexible polymers to membranes: Anomalous diffusion and reptation. *J Phys II* 7:1761–1788
- Guck J, Schinkinger S, Lincoln B, Wottawah F, Ebert S, Romeyke M, Lenz D, Erickson HM, Ananthkrishnan R, Mitchell D, Kas J, Ulvick S, Bilby C (2005) Optical deformability as an inherent cell marker for testing malignant transformation and metastatic competence. *Biophys J* 88:3689–3698. doi:[10.1529/biophysj.104.045476](https://doi.org/10.1529/biophysj.104.045476)
- Guigas G, Kalla C, Weiss M (2007) Probing the nanoscale viscoelasticity of intracellular fluids in living cells. *Biophys J* 93:316–323. doi:[10.1529/biophysj.106.099267](https://doi.org/10.1529/biophysj.106.099267)
- Guo Q, Park S, Ma HS (2012) Microfluidic micropipette aspiration for measuring the deformability of single cells. *Lab Chip* 12:2687–2695. doi:[10.1039/C2lc40205j](https://doi.org/10.1039/C2lc40205j)
- Head DA, Mizuno D (2010) Nonlocal fluctuation correlations in active gels. *Phys Rev E* 81:041910
- Heidemann SR, Wirtz D (2004) Towards a regional approach to cell mechanics. *Trends Cell Biol* 14:160–166. doi:[10.1016/j.tcb.2004.02.003](https://doi.org/10.1016/j.tcb.2004.02.003)
- Heilbronn A (1922) Eine neue Methode zur Bestimmung der Viskosität lebender Protoplasten
- Herrmann H, Bar H, Kreplak L, Strelkov SV, Aebi U (2007) Intermediate filaments: from cell architecture to nanomechanics. *Nat Rev Mol Cell Biol* 8:562–573. doi:[10.1038/Nrm2197](https://doi.org/10.1038/Nrm2197)
- Hiramoto Y (1969a) Mechanical properties of the protoplasm of the sea urchin egg. I. Unfertilized egg. *Exp Cell Res* 56:201–208
- Hiramoto Y (1969b) Mechanical properties of the protoplasm of the sea urchin egg. II. Fertilized egg. *Exp Cell Res* 56:209–218
- Hoffman BD, Massiera G, Van Citters KM, Crocker JC (2006) The consensus mechanics of cultured mammalian cells. *Proc Natl Acad Sci USA* 103:10259–10264. doi:[10.1073/pnas.0510348103](https://doi.org/10.1073/pnas.0510348103)
- Hou HW, Li QS, Lee GYH, Kumar AP, Ong CN, Lim CT (2009) Deformability study of breast cancer cells using microfluidics. *Biomed Microdevices* 11:557–564. doi:[10.1007/s10544-008-9262-8](https://doi.org/10.1007/s10544-008-9262-8)
- Huang S, Ingber DE (1999) The structural and mechanical complexity of cell-growth control. *Nat Cell Biol* 1:E131–E138
- Indei T, Schieber JD, Cordoba A (2012a) Competing effects of particle and medium inertia on particle diffusion in viscoelastic materials, and their ramifications for passive microrheology. *Phys Rev E* 85. doi:[10.1103/PhysRevE.85.041504](https://doi.org/10.1103/PhysRevE.85.041504)
- Indei T, Schieber JD, Cordoba A, Pilyugina E (2012b) Treating inertia in passive microbead rheology. *Phys Rev E* 85. doi:[10.1103/PhysRevE.85.021504](https://doi.org/10.1103/PhysRevE.85.021504)
- Janmey PA, Weitz DA (2004) Dealing with mechanics: mechanisms of force transduction in cells. *Trends Biochem Sci* 29:364–370. doi:[10.1016/j.tibs.2004.05.003](https://doi.org/10.1016/j.tibs.2004.05.003)
- Jeon JH, Tejedor V, Burov S, Barkai E, Selhuber-Unkel C, Berg-Sorensen K, Oddershede L, Metzler R (2011) In vivo anomalous diffusion and weak ergodicity breaking of lipid granules. *Phys Rev Lett* 106:048103. doi:[10.1103/PhysRevLett.106.048103](https://doi.org/10.1103/PhysRevLett.106.048103)
- Kahana A, Kenan G, Feingold M, Elbaum M, Granek R (2008) Active transport on disordered microtubule networks: The generalized random velocity model. *Phys Rev E Stat Nonlinear Soft Matter Phys* 78:051912
- King M, Macklem PT (1977) Rheological properties of microliter quantities of normal mucus. *J Appl Physiol* 42:797–802
- Kulic IM, Brown AE, Kim H, Kural C, Blehm B, Selvin PR, Nelson PC, Gelfand VI (2008) The role of microtubule movement in bidirectional organelle transport. *Proc Natl Acad Sci USA* 105:10011–10016. doi:[10.1073/pnas.0800031105](https://doi.org/10.1073/pnas.0800031105)
- Lau AWC, Hoffman BD, Davies A, Crocker JC, Lubensky TC (2003) Microrheology, stress fluctuations, and active behavior of living cells. *Phys Rev Lett* 91. doi:[10.1103/PhysRevLett.91.198101](https://doi.org/10.1103/PhysRevLett.91.198101)
- Leijnse N, Jeon JH, Loft S, Metzler R, Oddershede LB (2012) Diffusion inside living human cells. *Eur Phys J-Spec Top* 204:75–84. doi:[10.1140/epjst/e2012-01553-y](https://doi.org/10.1140/epjst/e2012-01553-y)
- Leoncini X, Kuznetsov L, Zaslavsky GM (2004) Evidence of fractional transport in point vortex flow. *Chaos Soliton Fract* 19:259–273. doi:[10.1016/S0960-0779\(03\)00040-7](https://doi.org/10.1016/S0960-0779(03)00040-7)
- Levine AJ, Lubensky TC (2000) One- and two-particle microrheology. *Phys Rev Lett* 85:1774–1777
- Li YX, Vanapalli SA, Duits MHG (2009) Dynamics of ballistically injected latex particles in living human endothelial cells. *Biorheology* 46:309–321. doi:[10.3233/Bir-2009-0542](https://doi.org/10.3233/Bir-2009-0542)
- Lim CT, Zhou EH, Li A, Vedula SRK, Fu HX (2006) Experimental techniques for single cell and single molecule biomechanics. *Mat Sci Eng C-Bio S* 26:1278–1288. doi:[10.1016/j.msec.2005.08.022](https://doi.org/10.1016/j.msec.2005.08.022)
- MacKintosh FC, Schmidt CF (1999) Microrheology. *Curr Opin Colloid In* 4:300–307. doi:[10.1016/S1359-0294\(99\)90010-9](https://doi.org/10.1016/S1359-0294(99)90010-9)
- Mason TG (2000) Estimating the viscoelastic moduli of complex fluids using the generalized Stokes–Einstein equation. *Rheol Acta* 39:371–378
- Mason TG, Dhople A, Wirtz D (1997a) Concentrated DNA rheology and microrheology. *MRS Proc Stat Mech Phys Biol* 463:153–158
- Mason TG, Ganesan K, vanZanten JH, Wirtz D, Kuo SC (1997b) Particle tracking microrheology of complex fluids. *Phys Rev Lett* 79:3282–3285
- Mason TG, Weitz DA (1995) Optical measurements of frequency-dependent linear viscoelastic moduli of complex fluids. *Phys Rev Lett* 74:1250–1253
- Mizuno D, Tardin C, Schmidt CF, MacKintosh FC (2007) Nonequilibrium mechanics of active cytoskeletal networks. *Science* 315:370–373. doi:[10.1126/science.1134404](https://doi.org/10.1126/science.1134404)
- Morse DC (1998) Viscoelasticity of concentrated isotropic solutions of semiflexible polymers. 2. Linear response. *Macromolecules* 31:7044–7067
- Nagle RB (1994) A review of intermediate filament biology and their use in pathological diagnosis. *Mol Biol Rep* 19:3–21
- Panorchan P, Lee JSH, Kole TP, Tseng Y, Wirtz D (2006) Microrheology and ROCK signaling of human endothelial cells embedded in a 3D matrix. *Biophys J* 91:3499–3507. doi:[10.1529/biophysj.106.084988](https://doi.org/10.1529/biophysj.106.084988)
- Pelling AE, Dawson DW, Carreon DM, Christiansen JJ, Shen RR, Teitell MA, Gimzewski JK (2007) Distinct contributions of microtubule subtypes to cell membrane shape and stability. *Nanomed-Nanotechnol* 3:43–52. doi:[10.1016/j.nano.2006.11.006](https://doi.org/10.1016/j.nano.2006.11.006)
- Pikovsky AS (1991) Statistical properties of dynamically generated anomalous diffusion. *Phys Rev A* 43:3146–3148
- Pollard TD, Cooper JA (2009) Actin, a central player in cell shape and movement. *Science* 326:1208–1212. doi:[10.1126/science.1175862](https://doi.org/10.1126/science.1175862)

- Puig-de-Morales M, Grabulosa M, Alcaraz J, Mullol J, Maksym GN, Fredberg JJ, Navajas D (2001) Measurement of cell microrheology by magnetic twisting cytometry with frequency domain demodulation. *J Appl Physiol* 91:1152–1159
- Qi D, Hoelzle DJ, Rowat AC (2012) Probing single cells using flow in microfluidic devices. *Eur Phys J-Spec Top* 204:85–101. doi:10.1140/epjst/e2012-01554-x
- Rahman A (1964) Correlations in the motion of atoms in liquid Argon. *Phys Rev* 136:A405–A411
- Raupach C, Zitterbart DP, Mierke CT, Metzner C, Muller FA, Fabry B (2007) Stress fluctuations and motion of cytoskeletal-bound markers. *Phys Rev E* 76:011918. doi:10.1103/PhysRevE.76.011918
- Rich JP, McKinley GH, Doyle PS (2011) Size dependence of microprobe dynamics during gelation of a discotic colloidal clay. *J Rheol* 55:273–299. doi:10.1122/1.3532979
- Robert D, Nguyen TH, Gallet F, Wilhelm C (2010) In vivo determination of fluctuating forces during endosome trafficking using a combination of active and passive microrheology. *PLoS ONE* 5. doi:10.1371/journal.pone.0010046
- Rogers SS, Waigh TA, Zhao XB, Lu JR (2007) Precise particle tracking against a complicated background: polynomial fitting with Gaussian weight. *Phys Biol* 4:220–227. doi:10.1088/1478-3975/4/3/008
- Rubinstein M, Colby RH (2003) *Polymer physics*. Oxford University Press, Oxford
- Savin T, Doyle PS (2005) Static and dynamic errors in particle tracking microrheology. *Biophys J* 88:623–638. doi:10.1529/biophysj.104.042457
- Saxton MJ (1993) Lateral diffusion in an archipelago—single-particle diffusion. *Biophys J* 64:1766–1780
- Saxton MJ, Jacobson K (1997) Single-particle tracking: applications to membrane dynamics. *Annu Rev Biophys Biomol Struct* 26:373–399
- Schwoebel ED, Ho TH, Moore MS (2002) The mechanism of inhibition of Ran-dependent nuclear transport by cellular ATP depletion. *J Cell Biol* 157:963–974. doi:10.1083/jcb.200111077
- Snider J, Lin F, Zahedi N, Rodionov V, Yu CC, Gross SP (2004) Intracellular actin-based transport: how far you go depends on how often you switch. *Proc Natl Acad Sci USA* 101:13204–13209. doi:10.1073/pnas.0403092101
- Squires TM, Brady JF (2005) A simple paradigm for active and nonlinear microrheology. *Phys Fluids* 17. doi:10.1063/1.1960607
- Squires TM, Mason TG (2010) Fluid mechanics of microrheology. *Annu Rev Fluid Mech* 42:413–438. doi:10.1146/annurev-fluid-121108-145608
- Stuhrmann B, Soares e Silva M, Depken M, MacKintosh FC, Koenig GH (2012) Nonequilibrium fluctuations of a remodeling in vitro cytoskeleton. *Phys Rev E* 86:020901
- Suh JH, Wirtz D, Hanes J (2004) Real-time intracellular transport of gene nanocarriers studied by multiple particle tracking. *Biotechnol Prog* 20:598–602. doi:10.1021/bp034251y
- Suresh S (2007) Biomechanics and biophysics of cancer cells. *Acta Biomater* 3:413–438. doi:10.1016/j.actbio.2007.04.002
- Suresh S, Spatz J, Mills JP, Micoulet A, Dao M, Lim CT, Beil M, Seufferlein T (2005) Connections between single-cell biomechanics and human disease states: gastrointestinal cancer and malaria. *Acta Biomater* 1:15–30. doi:10.1016/j.actbio.2004.09.001
- Sutherland W (1905) A dynamical theory of diffusion for non-electrolytes and the molecular mass of albumin. *Philos Mag* 9:781–785
- Tanase M, Biaisi N, Sheetz M (2007) Magnetic tweezers in cell biology. *Method Cell Biol* 83:473–493. doi:10.1016/S0091-679x(07)83020-2
- Thoumine O, Ott A, Cardoso O, Meister JJ (1999) Microplates: a new tool for manipulation and mechanical perturbation of individual cells. *J Biochem Biophys Methods* 39:47–62
- Toyota T, Head DA, Schmidt CF, Mizuno D (2011) Non-Gaussian athermal fluctuations in active gels. *Soft Matter* 7:3234–3239. doi:10.1039/C0sm00925c
- Tseng Y, Kole TP, Wirtz D (2002) Micromechanical mapping of live cells by multiple-particle-tracking microrheology. *Biophys J* 83:3162–3176
- Tseng Y, Lee JSH, Kole TP, Jiang I, Wirtz D (2004) Microorganization and visco-elasticity of the interphase nucleus revealed by particle nanotracking. *J Cell Sci* 117:2159–2167. doi:10.1242/jcs.01073
- Umansky M, Weihs D (2012) Novel algorithm and MATLAB-based program for automated power law analysis of single particle, time-dependent mean-square displacement. *Comput Phys Commun* 183:1783–1792. doi:10.1016/j.cpc.2012.03.001
- Valentine MT, Kaplan PD, Thota D, Crocker JC, Gislis T, Prud'homme RK, Beck M, Weitz DA (2001) Investigating the microenvironments of inhomogeneous soft materials with multiple particle tracking. *Phys Rev E* 64:061506. doi:10.1103/Phys-reve.64.061506
- Valiron O, Caudron N, Job D (2001) Microtubule dynamics. *Cell Mol Life Sci* 58:2069–2084
- Van Citters KM, Hoffman BD, Massiera G, Crocker JC (2006) The role of F-actin and myosin in epithelial cell rheology. *Biophys J* 91:3946–3956. doi:10.1529/biophysj.106.091264
- Van Hove L (1954) Correlations in space and time and born approximation scattering in systems of interacting particles. *Physical Review* 95:249–262
- Van Vliet KJ, Bao G, Suresh S (2003) The biomechanics toolbox: experimental approaches for living cells and biomolecules. *Acta Mater* 51:5881–5905. doi:10.1016/j.actamat.2003.09.001
- Weber SC, Spakowitz AJ, Theriot JA (2010) Bacterial chromosomal loci move subdiffusively through a viscoelastic cytoplasm. *Phys Rev Lett* 104:238102. doi:10.1103/Physrevlett.104.238102
- Weeks ER, Crocker JC, Levitt AC, Schofield A, Weitz DA (2000) Three-dimensional direct imaging of structural relaxation near the colloidal glass transition. *Science* 287:627–631
- Weihs D, Gilad D, Seon M, Cohen I (2012) Image-based algorithm for analysis of transient trapping in single-particle trajectories. *Microfluid Nanofluid* 12:337–344. doi:10.1007/s10404-011-0877-3
- Weihs D, Mason TG, Teitell MA (2006) Bio-microrheology: a frontier in microrheology. *Biophys J* 91:4296–4305. doi:10.1529/biophysj.106.081109
- Weihs D, Mason TG, Teitell MA (2007a) Effects of cytoskeletal disruption on transport, structure, and rheology within mammalian cells. *Phys Fluids* 19. doi:10.1063/1.2795130
- Weihs D, Teitell MA, Mason TG (2007b) Simulations of complex particle transport in heterogeneous active liquids. *Microfluid Nanofluid* 3:227–237. doi:10.1007/s10404-006-0117-4
- Weiss M, Elsner M, Kartberg F, Nilsson T (2004) Anomalous subdiffusion is a measure for cytoplasmic crowding in living cells. *Biophys J* 87:3518–3524. doi:10.1529/biophysj.104.044263
- Wilhelm C (2008) Out-of-equilibrium microrheology inside living cells. *Phys Rev Lett* 101:028101. doi:10.1103/Phys-revlett.101.028101
- Willenbacher N, Oelschlaeger C, Schopferer M, Fischer P, Cardinaux F, Scheffold F (2007) Broad bandwidth optical and mechanical rheometry of wormlike micelle solutions. *Phys Rev Lett* 99. doi:10.1103/Physrevlett.99.068302
- Xu JY, Viasnoff V, Wirtz D (1998) Compliance of actin filament networks measured by particle-tracking microrheology and diffusing wave spectroscopy. *Rheol Acta* 37:387–398

- Yagi K (1961) The mechanical and colloidal properties of Amoeba protoplasm and their relations to the mechanism of amoeboid movement. *Comp Biochem Physiol* 3:73–91
- Yamada S, Wirtz D, Kuo SC (2000) Mechanics of living cells measured by laser tracking microrheology. *Biophys J* 78:1736–1747
- Yizraeli ML, Weihs D (2011) Time-dependent micromechanical responses of breast cancer cells and adjacent fibroblasts to electric treatment. *Cell Biochem Biophys* 61:605–618. doi:[10.1007/s12013-011-9244-y](https://doi.org/10.1007/s12013-011-9244-y)
- Zemel A, Rehfeldt F, Brown AEX, Discher DE, Safran SA (2010) Optimal matrix rigidity for stress-fibre polarization in stem cells. *Nat Phys* 6:468–473. doi:[10.1038/Nphys1613](https://doi.org/10.1038/Nphys1613)
- Zhang H, Liu KK (2008) Optical tweezers for single cells. *J R Soc Interface* 5:671–690. doi:[10.1098/rsif.2008.0052](https://doi.org/10.1098/rsif.2008.0052)